Piezoresistive 3D graphene-PDMS spongy pressure sensors for IoT enabled wearables and smart products

Sengupta, Debarun; Kamat, Amar M; Smit, Quinten; Jayawardhana, Bayu; Kottapalli, Ajay Giri Prakash

Published in:
Flexible and Printed Electronics

DOI:
10.1088/2058-8585/ac4d0e

Publication date:
2022

Flexible and Printed Electronics

Piezoresistive 3D graphene-PDMS spongy pressure sensors for IoT enabled wearables and smart products

To cite this article before publication: Debarun Sengupta *et al* 2022 *Flex. Print. Electron.* in press https://doi.org/10.1088/2058-8585/ac4d0e

IOP Publishing Flexible and Printed Electronics
Flex. Print. Electron. **XX** (XXXX) XXXXXX https://doi.org/XXXX/XXXX

Piezoresistive 3D graphene-PDMS spongy pressure sensors for IoT enabled wearables and smart products

Debarun Sengupta [1], Amar M. Kamat [1], Quinten Smit [1], Bayu Jayawardhana[2] and Ajay Giri Prakash Kottapalli [1,3]

[1] Department of Advanced Production Engineering, Faculty of Science and Engineering, University of Groningen, Groningen, The Netherlands;
[2]Discrete Technology and Production Automation, Engineering and Technology Institute Groningen, Faculty of Science and Engineering, University of Groningen, The Netherlands
[23]MIT Sea Grant College Program, Massachusetts Institute of Technology, Cambridge, USA
E-mail:a.g.p.kottapalli@rug.nl

Received xxxxxx
Accepted for publication xxxxxx
Published xxxxxx

Abstract

Recently, 3D porous graphene-polymer composite-based piezoresistive sensors have gained significant traction in the field of flexible electronics owing to their ultralightweight nature, high compressability, robustness, and excellent electromechanical properties. In this work, we present an improved facile recipe for developing repeatable, reliable, and linear 3D graphene-PDMS spongy sensors for internet of things (IoT)-enabled wearable systems and smart consumer products. Fundamental morphological characterization and sensing performance assessment of the piezoresistive 3D graphene-polymer sensor were conducted to establish its suitability for the development of squeezable, flexible, and skin-mountable human motion sensors. The density and porosity of the sponges were determined to be 250 mg cm^{-3} and 74 % respectively. Mechanical compressive loading tests conducted on the sensors revealed an average elastic modulus as low as ~56.7 kPa. Dynamic compressive force-resistance change response tests conducted on four identical sensors revealed a linear piezoresistive response (in the compressive load range 0.42 – 2.18 N) with an average force sensitivity of 0.3470 ± 0.0794 N^{-1}. In addition, an accelerated lifetime test comprising 1500 compressive loading cycles (at 3.90 N uniaxial compressive loading) was conducted to demonstrate the long-term reliability and stability of the sensor. To test the applicability of the sensors in smart wearables, four identical graphene-PDMS sponges were configured on the fingertip regions of a soft nitrile glove to develop a pressure sensing smart glove for real-time haptic pressure monitoring. Similarly, the sensors were also integrated into the Philips 9000 series electric shaver to realize smart shaving applications with the ability to monitor shaving motions. Furthermore, the readiness of our system for next-generation IoT-enabled applications was demonstrated by integrating the smart glove with an embedded system software utilizing the an open source microcontroller platform. The system was capable of identifying real-time qualitative pressure distribution across the fingertips while grasping daily life objects, thus establishing the suitability of such sensors for next-generation wearables for prosthetics, consumer devices, and personalized healthcare monitoring devices.

Keywords: piezoresistive; graphene; sensors; wearables

1. Introduction

With the rising demand for minimally invasive wearable healthcare monitoring devices, significant advances on wearable devices have been made over the past two decades across the globe that are based on the use of advanced materials and MEMS fabrication technologies. Facile fabrication of wearable sensors can alleviate a number of bottlenecks associated with conventional inertial measurement unit (IMU) based activity trackers. For instance, flexible sensors integrated in smart wearables can provide a host of information regarding gait characteristics, grasping ability in patients suffering from progressive nervous system disorders like Parkinson's disease, and other neurological conditions related muscle tremors and twitching. Furthermore, skin-mountable, flexible, and ultralightweight sensors can potentially enable the development of next generation prosthetic devices for recreating the sense of touch in myoelectric prosthesis and soft skin-like sensors applicable to intelligent human-machine interfaces.

Most flexible and wearable pressure/strain sensors reported in the literature transduce an external pressure stimulus to an electrical signal via capacitive [1,2], piezoresistive [3–6], piezoelectric [7–9], and triboelectric mechanisms [10,11]. The sensors intended for wearable applications need to be ultralightweight, robust, inexpensive yet reliable in order to withstand wear caused by daily activities without compromising the performance. Furthermore, a simple and repeatable manufacturing method is highly desired for systems utilizing multiple sensors in parallel for human motion monitoring and smart soft-robotics applications.

In the past, several research groups have utilized the piezoresistive properties of semiconductors, polymer-nanomaterial composites, and metallic strain gauges for developing wearable sensors. In particular, polymer-nanomaterial composites have attracted significant interest in the research community owing to their ultralightweight nature and the ability to withstand large deformation without failing which make them suitable for wearable device applications. Typically, polymer-nanomaterial composite based piezoresistive sensors are comprised of soft polymer materials like polydimethylsiloxane (PDMS), polyurethane (PU), polyimide (PI), and Ecoflex which act as the elastomeric insulating bases owing to their excellent flexibility, stretchability and responsiveness to torsion and mechanical deformation [12–16]. 0D nanomaterials like carbon black [17], 1D nanomaterials like carbon nanofibers [4,18], silver nanowires (AgNWs) [14,19], carbon nanotubes (CNTs) [15,20], and 2D nanomaterials like graphene [3,6,21,22] and MXene [23,24] have been investigated extensively for developing piezoresistive sensors. Of all the nanomaterial fillers, graphene (a 2-d allotrope of carbon comprised of sp^2 hybridized carbon arranged in a planar honeycomb fashion) has drawn much interest of flexible electronics community owing to its excellent electromechanical properties. Graphene in its natural state is a 2D material and can be transformed into a more desirable three-dimensional (3D) form which facilitates its use in applications which involving large stress and deformation. In addition, 3D porous structure enables the fabrication of ultra-lightweight, compressive, and breathable sensors. In a broad sense, the four most common configurations of 3D graphene, viz. sponges [14,25], foams [22,26], lattices [27], and aerogels [28], have been widely reported in the literature. Various methods for achieving porous 3D graphene-based piezoresistive sensors including template based synthesis, self-assembly, 3D printing, and electrospinning have been reported in the literature [29]. Among the aforementioned methods, templating method is particularly attractive owing to its simplicity and process scalability. Qin et al. reported reduced graphene oxide PI nanocomposite-based ultra-lightweight, stretchable, and compressible piezoresistive strain sensors [22]. Taking a slightly different approach, Pang et al. reported a process of fabricating graphene-PDMS nanoporous sensors using chemical vapor deposition (CVD)-grown graphene on foamy nickel template, subsequent infiltration of the pores with PDMS prepolymer, curing, and finally etching the nickel template using hydrochloric acid to form the 3D spongy structure [3]. Various other methods including dip-coating PU and PDMS spongy structures in graphene suspension to form 3D porous graphene structures have been reported [30–32]. In the past, we have reported a facile method of developing graphene-PDMS spongy sensors through PDMS sugar-scaffolding and subsequent dip coating in graphene nanoplatelet suspension and drying for consecutive six cycles [6,33]. Most of the sensors reported in literature suffer from non-linear strain-piezoresistive response characteristics [6,26,34,35]. Furthermore, process repeatability and long term reliability of the manufactured sensors are two critical aspects often overlooked in literature.

In this work, we report an improved facile method for fabricating graphene-PDMS sponges for internet of things (IoT) enabled wearable applications. In contrast to our previous work [6], the number of dip-coating cycles to load the PDMS sponges have been reduced (three cycles), thus reducing the overall graphene consumption by 50%. The dip coated sponges are dried at a relatively higher temperature of 120˚C which overcures the PDMS sponges and in the process might help bind the graphene nanoflakes to the inner pore walls of the PDMS sponges. The ultra-lightweight nature of the graphene-PDMS sponge is reflected by its density of ~250 mg cm^{-3}. Cyclic compressive loading tests (up to 70% compressive strain) conducted on the graphene-PDMS sponge revealed an average elastic modulus of ~56.7 kPa. Dynamic compressive uniaxial loading piezoresistive response tests (up

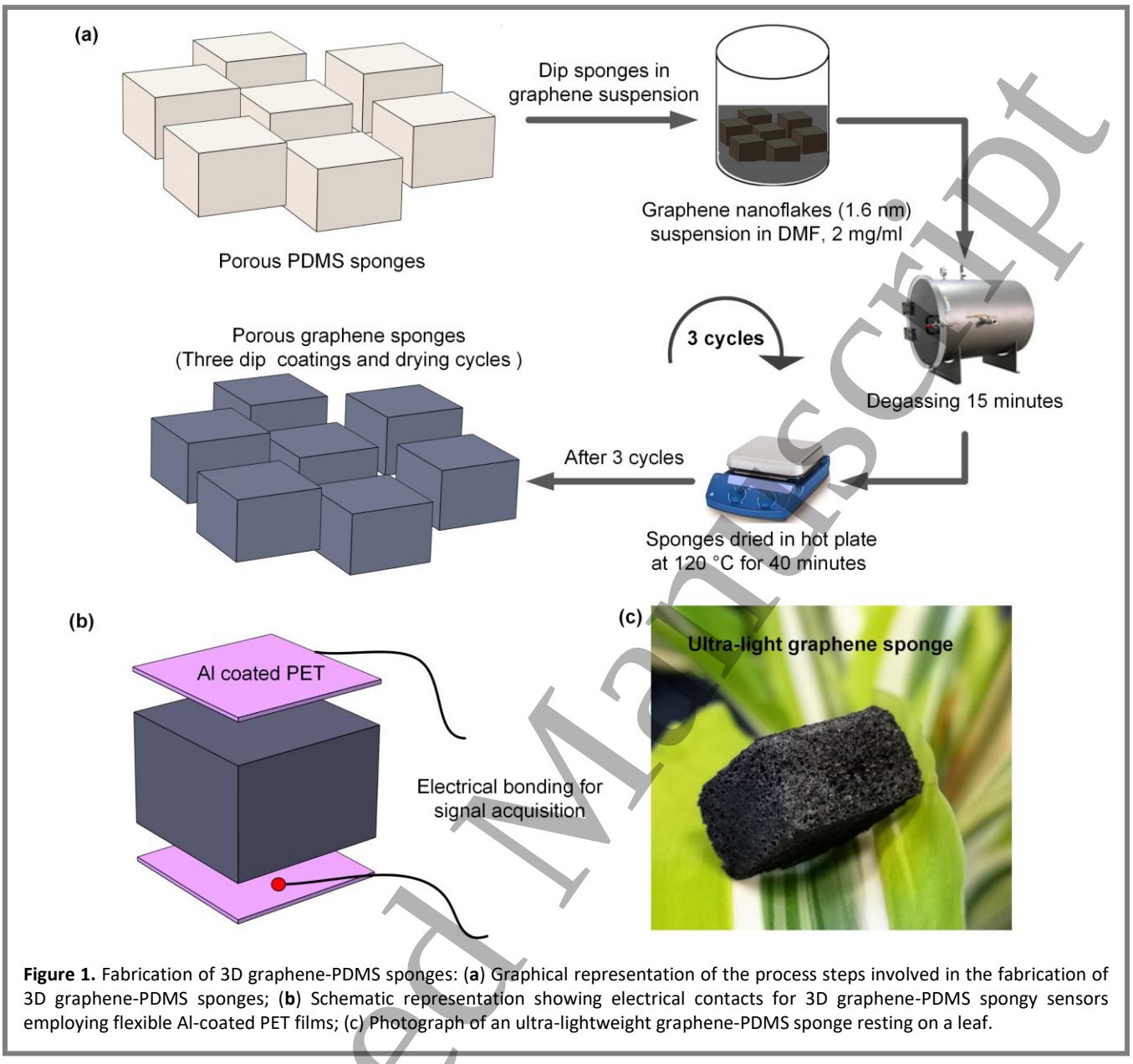

Figure 1. Fabrication of 3D graphene-PDMS sponges: (**a**) Graphical representation of the process steps involved in the fabrication of 3D graphene-PDMS sponges; (**b**) Schematic representation showing electrical contacts for 3D graphene-PDMS spongy sensors employing flexible Al-coated PET films; (c) Photograph of an ultra-lightweight graphene-PDMS sponge resting on a leaf.

to 8.23 N load) conducted on the sensor revealed force sensitivities of 0.3068 N^{-1} , 0.2389 N^{-1} and 0.2451 N^{-1} at 0.1, 0.2, and 0.3 Hz frequencies respectively with a linear behavior in the compressive load range ~ 0.42 – 2.18 N. To demonstrate the repeatability of the fabrication process, electromechanical characterization experiments were conducted on four sensor samples and the average force sensitivities of the sensors was determined as 0.3470 ± 0.0794 N^{-1} at 0.2 Hz cyclic compressive loading with a linear response in the load range ~0.42 – 2.18 N. The linear compressive load piezoresistive response characteristics in the aforementioned load range makes the sensors particularly relevant for applications in werable devices for measuring haptic force and consumer products like smart shavers capable of providing active feedback to users for comfortable shaving experience [36,37]. Furthermore, accelerated lifetime tests consisting of 1500 compressive loading cycles (at 3.90 N load) was conducted to demonstrate the long-term reliability and stability of the sensor.

In order to demonstrate the feasibility of the graphene-PDMS sponges for applications in wearables, a smart glove with four identical sensors secured on the fingertip region was developed and various daily life objects were grasped wearing the glove while monitoring the relative pressure distribution across the fingertips. The sensors were also integrated into the Philips 9000 series electric shaver to demonstrate their application in smart shaving. Finally, to demonstrate the readiness of our sensors for IoT-enabled

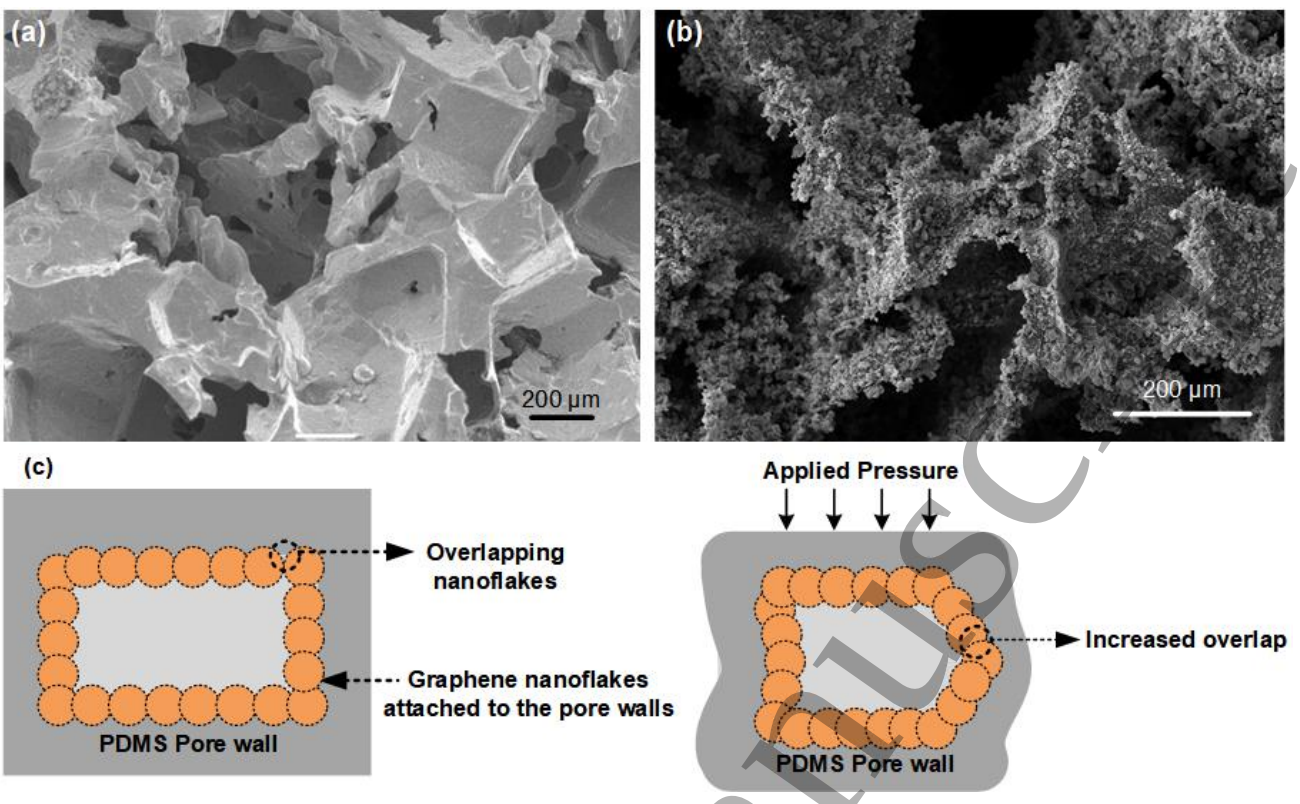

Figure 2. SEM micrographs of the blank and MLG nanoflakes loaded PDMS sponges: (**a**) Micrograph showing the blank PDMS sponge; (**b**) Micrographs showing the MLG nanoflakes loaded PDMS sponge; (c) Schematic representation of working mechanism of the piezoresistive graphene-PDMS sponges.

applications, an embedded system comprising of the smart glove with readout voltage divider circuits and with an open-source microcontroller development board of Arduino Uno is developed and demonstrated. Ultralightweight, repeatable, and robust sensors such as the ones demonstrated in this work could further guide the development of a future class of facile, accurate yet inexpensive wearable sensors for next generation prosthetic devices and intelligent human-machine interfaces.

2. Experimental Methodology

2.1 Fabrication of 3D graphene-PDMS sponges

A facile method for developing graphene-PDMS sponges was reported in our earlier works [6,33]. In the present work, we propose a modified fabrication method entailing PDMS sponges developed by sugar template scaffolding method loaded with multilayer graphene nanoflakes (~ 1.6 nm thick) (acquired from Graphene Supermarket, USA). Figure 1 schematically represents the process steps involved in the fabrication of the graphene-PDMS sponges. A homogenous suspension of multilayer graphene (MLG) nanoflakes was prepared by dispersing 50 mg of MLG nanoflakes in 25 ml N,N-Dimethyl formamide followed by sonication for a duration of 1 hour. The PDMS sponges were immersed in a beaker of the freshly prepared homogenous MLG graphene suspension. The beaker was then placed inside a vacuum desiccator and degassed for 10 minutes such that graphene nanoflakes can percolate and get evenly distributed across the innermost pores of the PDMS spongy base. Following the degassing step, the MLG loaded PDMS sponges were dried in a hot plate at 120 ˚C for 40 minutes. The relatively high temperature drying step further cures the PDMS sponges and in the process might help bind the MLG nanoflakes to the inner pore walls of the PDMS sponges. The dip coating and drying cycle was repeated thrice unlike in our previous work wherein the cycles were repeated for six times. The lesser number of dip coating cycles help in reducing the overall graphene consumption, thus leading to almost fifty percent reduction in materials cost. In order to develop pressure sensors from the graphene-PDMS sponges, aluminum coated polyethylene terephthalate (PET) films were attached to the two ends of the sponges using bare conductive carbon ink as schematically represented in figure 1b. Thin single strand copper wires were attached to the conductive ends of the

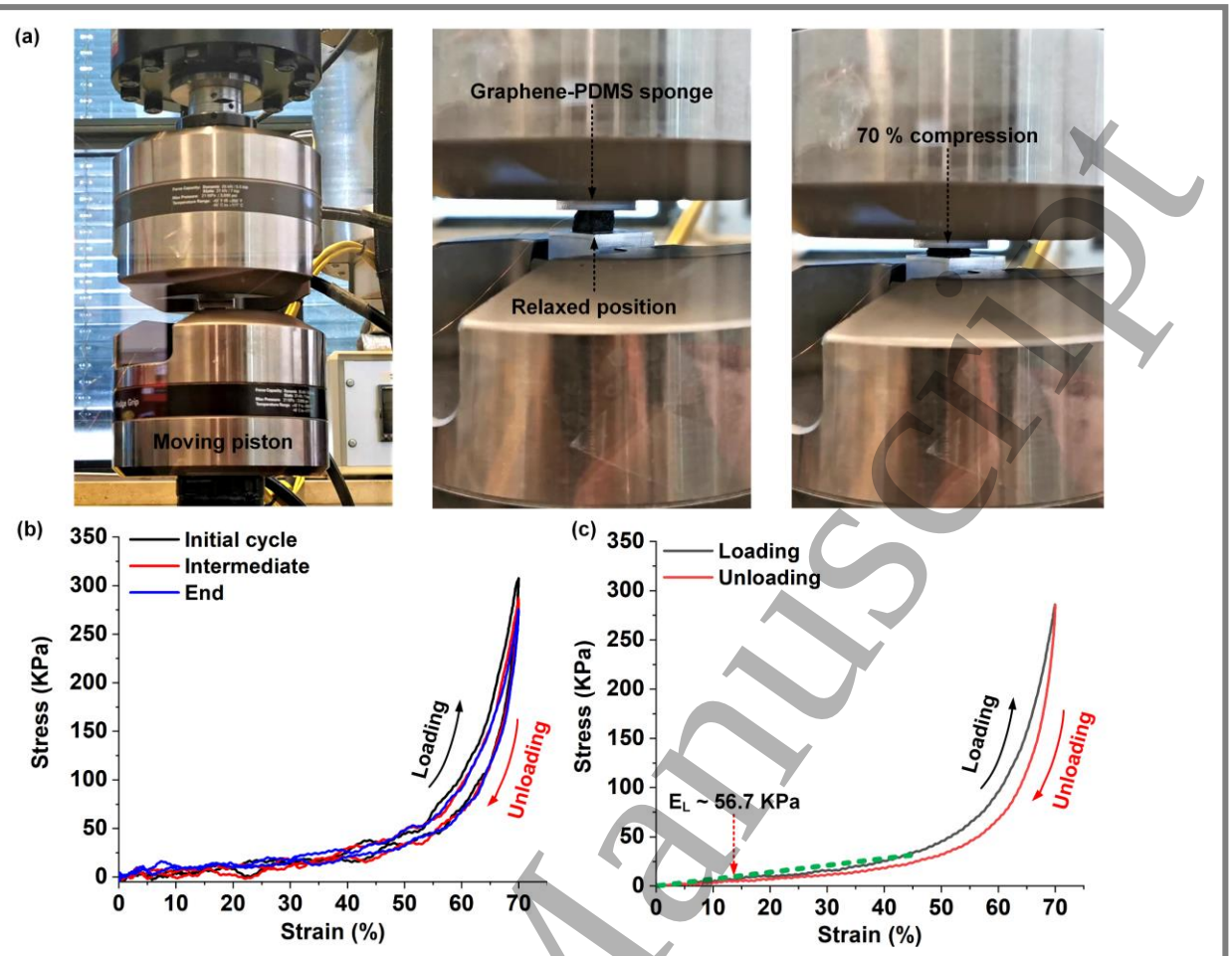

Figure 3. Mechanical characterization of graphene-loaded PDMS sponge: (**a)** Photographs of the experimental setup employed for mechanical characterization of the graphene-loaded PDMS sponge; (**b**) Plot showing stress-strain characteristics for three loading-unloading cycles chosen from the beginning, middle, and end of the experiment; (c) Stress-strain curve for the graphene-PDMS sponge averaged over 48 cycles of periodic compression test and smoothed; linear regression in the strain range 0-45 % reveals an average elastic modulus of 56.7 KPa.

flexible electrodes for electrical connection. Figure 1c shows an unbonded ultralightweight graphene-PDMS sponge resting on a leaf, demonstrating its ultralightweight nature.

2.2 Morphological characterization and sensing mechanism

A Tescan LYRA field-emission scanning electron microscope (FE-SEM) was employed to observe the morphological properties of both the unloaded and MLG nanoflakes loaded PDMS sponges. The samples were secured on appropriate SEM stubs and sputter coated with 10 nm layer of gold before conducting the imaging studies.

The SEM micrograph in figure 2a shows a blank as-prepared PDMS sponge. The porosity of the graphene-PDMS sponge was calculated as ~74 % using the formula: $1 - \frac{\rho_{sponge}}{\rho_{PDMS}}$; where ρ_{sponge} = 250 mg cm^{-3} is the density of the PDMS sponge and ρ_{PDMS} = 965 mg cm^{-3} is the known density [38] of bulk PDMS. The micrograph clearly indicates the microporous nature of the as prepared spongy base. The micrograph in figure 2b shows the MLG nanoflakes loaded PDMS sponge. As observed in the micrograph, graphene nanoflakes are attached to the inner pore walls of the PDMS sponges forming a dense percolation network allowing for a conductive path for charge carriers. In our previous works, mechanism behind the piezoresistive sensing of similar graphene-PDMS sponges has been hypothesized [33,39]. Figure 2c schematically represents the piezoresistive sensing principle underlying the sensors. The overlapping graphene nanoflakes attached to the inner pore walls form a dense percolation network resistance path for charge carriers. Upon application of an external pressure stimulus, densification of the sponge causes an overall increase in overlap between the nanoflakes subsequently leading to a decreased resistance of the MLG nanoflake percolation network which explains the stress induced resistance modulation of the graphene-PDMS sponges.

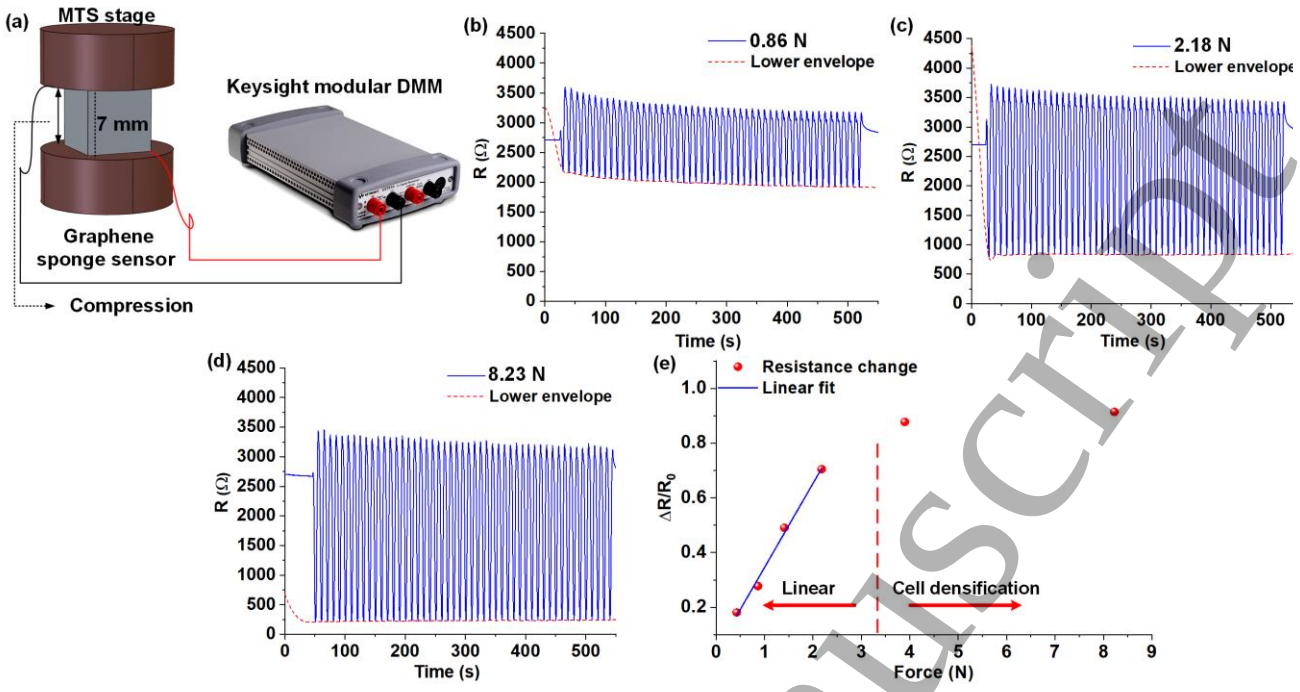

Figure 4. Electromechanical characterization of graphene-PDMS spongy sensors: (**a**) Schematic representation of the experimental setup employed for determining the sensitivity of the sensors; (**b**) – (**d**) Resistance change responses of the sensor for 50 cycles of three different uniaxial compressive loads (0.86 N, 2.18 N, and 8.23 N); (**e**) Plot showing normalized resistance change versus applied uniaxial compressive loads on the sensor.

2.3 Experimental setup for gauge factor and repeatability characterization

For characterizing the compressive force sensitivity, repeatability demonstration, and accelerated lifetime performance evaluation, the MTS 810 uniaxial testing setup was employed. Figure 3a schematically represents the setup employed for the electromechanical characterization experiments. The graphene-PDMS spongy sensor measuring 1 x 1 x 0.7 cm (l x b x h) was secured with a double-sided tape to the bottom piston of the machine. For the experiment involving compressive load sensitivity characterization, the movable piston was programmed to move at various fixed distances (0.7, 1.4, 2.1, 2.8, 3.5, and 4.2 mm) in a sinusoidal fashion to apply cyclic compressive tactile force in the range ~ 0.4 - 8N. The graphene-PDMS sponge (Sensor 1) was subjected to a series of 50 uniaxial loading up to 70% compressive strain (~ 4.9 mm displacement) to extract the Force-displacement characteristics. The relation between the displacement and force is averaged for 50 cycles. The average value of force (for each individual displacement step) is reported and considered for calculating the force sensitivity. The baseline drift which might arise due to settling of graphene nanoflakes in the inner pore walls of the PDMS sponge affects the force resistance change response of the sensor. It is assumed that the initial break-in phenomenon is unlikely to change the force displacement relation of the sensor over successive repetitions of the experiments.

2.4 Data acquisition setup

For the experiments involving the compressive load sensitivity characterizations and repeatability assessment, Keysight U2741a modular digital multimeter (DMM) was employed. The sensors were connected to the DMM and the data was continuously logged in the Keysight BenchVue software.

The resistances of the graphene-PDMS sponges developed in this work lie in the range ~ 2.5 – 3.5 kΩ; and consequently, voltage divider circuits comprising the sensors and 0 − 5 kΩ variable resistors were employed for the experiments involving pressure sensing smart glove and accelerated lifetime performance evaluation. The unamplified voltage outputs from the voltage divider circuits were continuously acquired using a National Instruments data acquisition card (NI-DAQ UBS-6009) and logged using the NI Signal Express software at a sampling rate of 100 Hz. A Wheatstone bridge arrangement was used for the sensorized shaver experiments.

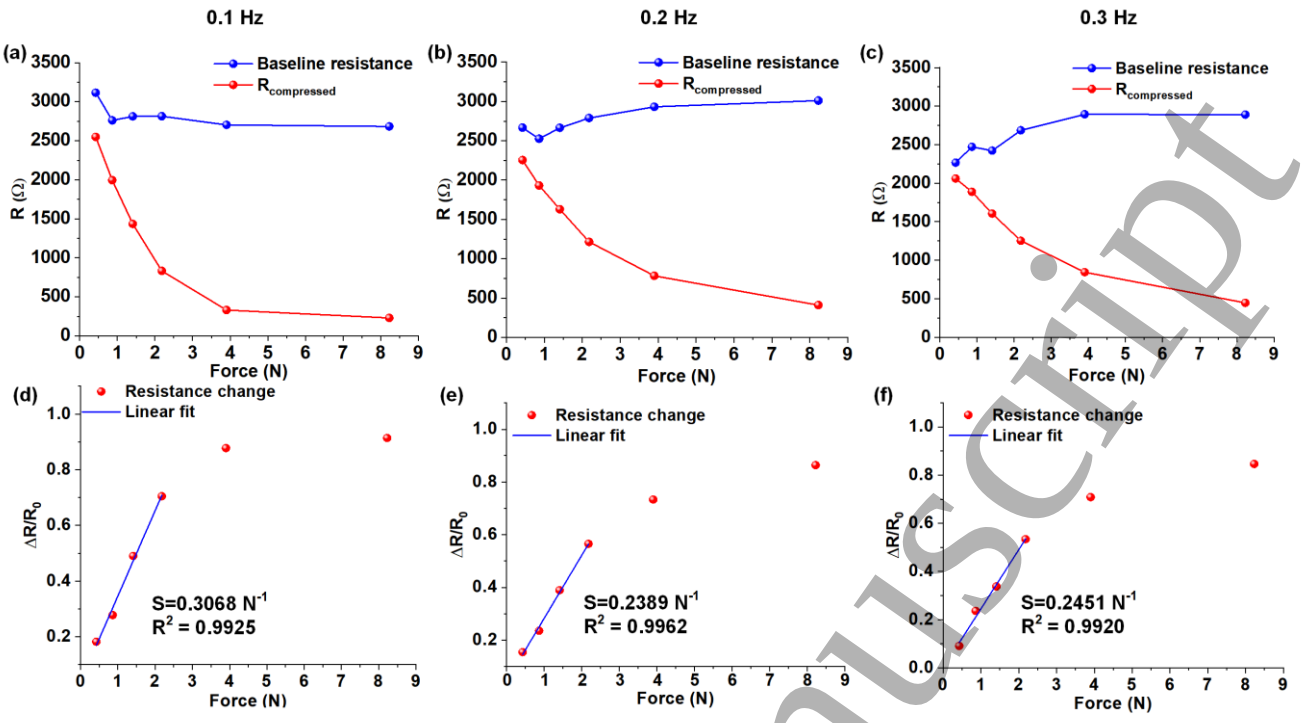

Figure 5. Force sensitivity and baseline resistance plots of the graphene-PDMS sponges for three different frequencies: (**a**) - (c) Plots showing absolute resistance versus applied uniaxial compressive loads along with the overall baseline resistance change for three different frequencies; (d) – (f) Plots showing the normalized resistance change of the sensor versus applied uniaxial compressive loads for three different frequencies.

3. Results

3.1 Electromechanical characterization of the 3D graphene-PDMS spongy sensors

To understand the compressibility and structural robustness of the fabricated graphene-PDMS sponges, the structure was subjected to 50 cycles of periodic compressive loading and unloading (up to 70 % compressive strain) at 0.1 Hz frequency using the MTS 810 compression stage as shown by the photographs in figure 3a. The force-displacement data was logged continuously employing an inbuilt load-cell accompanying the system. The results from the test were plotted in terms of compressive stress in the sponge as a function of strain from three distinct cycles picked from the beginning, middle and end of the periodic compressive strain loading test. Tests conducted on similar sensors in the past have revealed three distinct regions in the stress-strain characteristics, namely: a linear elastic region, stress plateau, and cell densification regime [22]. The plot in figure 3b shows the stress-strain characteristics curve for three cycles (chosen from the beginning, middle and end) of the periodic strain loading tests. As observed from the plots, the graphene-PDMS sensors shows a linear elastic behavior for strains less than 45 % followed by a cell densification regime. As opposed to a clear plateau region observed for similar sensors in the strain range 10-40% [22], the graphene-PDMS sponge developed in this work does not show a distinct plateau region. This observation agrees with the case of a 3D printed body centered cubic (BCC) flexible lattice reported by Kamat et al. [27] where the linear elastic region merges with the plateau region in the strain range ~ 0 – 50 % after which cell densification sets in. Furthermore, the hysterysis loop observed from the stress-strain characteristics curve signifies the viscoelastic nature of the graphene-PDMS sponge. The elastic modulus of the graphene-PDMS sponge was estimated to be ~56.7 kPa (averaged over 48 cycles of periodic cyclic strain test and smoothed) obtained from the slope of the stress-strain curve in the linear elastic regime as shown in the plot in figure 3c. From Gibson-Ashby model, for lattice and foamy structures (bending-dominated) [40]: $\frac{E_{Sponge}}{E_{PDMS}} = C\left(\frac{\rho_{Sponge}}{\rho_{PDMS}}\right)^2$; where, E_{sponge} = 56.7 kPa is the elastic modulus of the garphene-PDMS foam, E_{PDMS} = 2.61 MPa is the elastic modulus of PDMS (10:1, base:curing agent)[41], ρ_{sponge} and ρ_{PDMS} are the densities of the sponge and PDMS (sponge maetrial) respectively. From the model, the coeffcient 'C' was calculated as 0.3237 which lies with the expected range 0 – 2 reported for open foam and lattice structures [27,42]. From the stress-strain characteristics curve it can be concluded that the sensor should demonstrate a predictable linear resistance

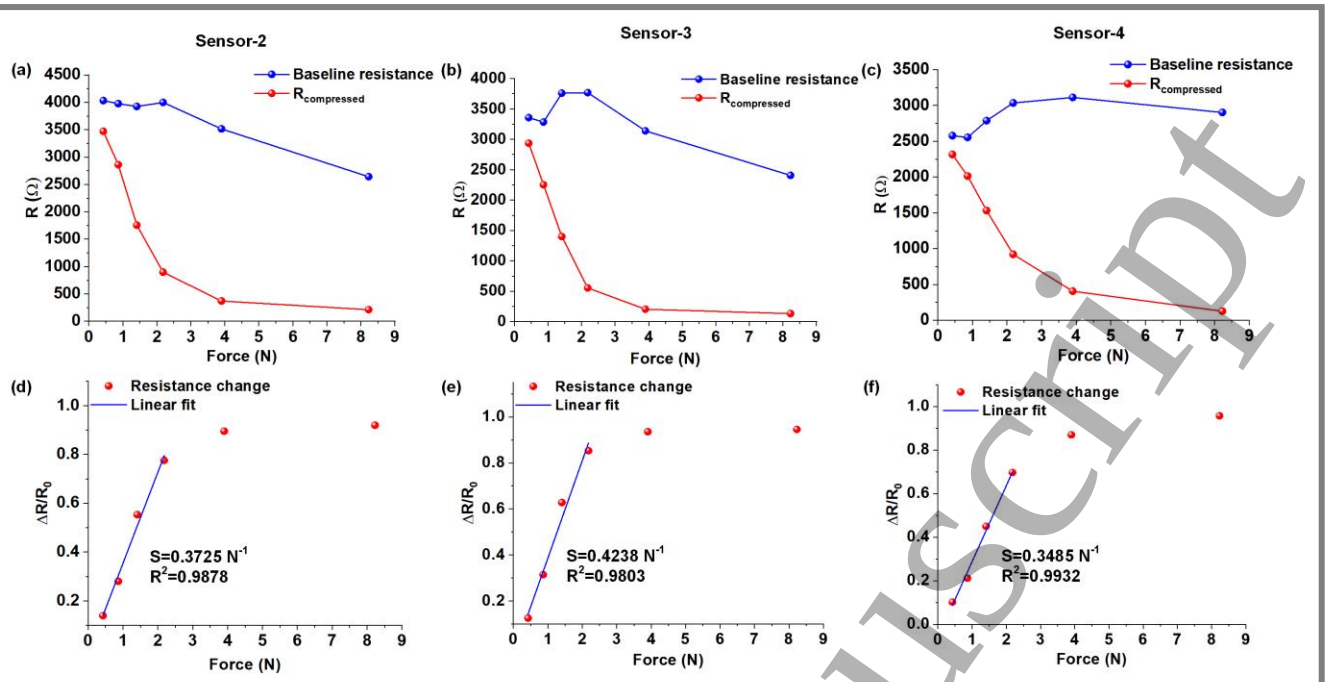

Figure 6. Force sensitivity and baseline resistance plots of three additional graphene-PDMS sponges for at 0.2 Hz cyclic stimulus: (a) - (c) Plots showing absolute resistance versus applied load along with the overall baseline resistance change for the three additional sensors; (d) – (f) Plots showing the normalized resistance change of the three sensors versus applied cyclic uniaxial compressive loading at 0.2 Hz.

change response for compressive strains up to 40% or equivalent uniaxial compressive loading upto ~ 2.18 N.

In this work, four different sensors were characterized for their individual force sensitivities to understand the repeatability of our fabrication process. In the first experiment, a sinusoidal loading-unloading test comprising of 50 cycles at 0.1 Hz was conducted on Sensor 1 to determine its sensitivity. The resistance change response of the sensor was continuously monitored utilizing Keysight U2741a DMM and the accompanying Benchvue software. The plots in figure 4b-d show the absolute resistance change response of the sensor for three uniaxial compressive loads of 0.86 N, 2.18 N, and 8.23 N respectively. Interestingly, the sensors show an initial drop in conductivity (increase in resistance) followed by an increase in conductivity with increasing load. This phenomenon is manifested as overshooting behavior of the resistance response plots in figure 4b-d. This behavior has been observed by Wu et al. [43] and Kamat et al. [27] previously and possible reason behind this peculiar behaviour could be attributed to increasing contact separation gap between adjacent MLG nanoflakes under lower loading conditions followed by recontacting of the adajacent graphene domains once the load crosses a certain load threshold. For calculating the normalized resistance change of the sensor, the following equation was used:

$$\frac{\Delta R}{R_0} = \frac{\Delta R}{R_{baseline}} = \frac{R_{baseline} - R_{compressed}}{R_{baseline}}$$

where, $R_{baseline}$ is calculated as the mean resistance of the sensor recorded at the beginning and end of an indvidual uniaxial loading-unloading series comprising of 50 cycles and $R_{compressed}$ is determined by drawing the lower envelopes of the response plots and calculating the mean resistance of the sensor under various compressive loading. The normalized resistance change versus compressive loading in the sponge was plotted and subsequent linear regression (with R-squared value 0.9926 in the load range ~ 0.42 – 2.18 N) conducted revealed a force sensitivity of 0.3068 N^{-1} as shown in figure 4e. As clearly observed from the plot in figure 4e, the sensor shows a linear response for uniaxial loading up to ~ 2.18 N in contrast to our previous work, where the sensor demonstrated a non-linear behavior in the same range [6]. The improved linearity in comparsion to our previous work can possibly be attributed to lesser graphene loading and drying step conducted at a relatively higher temperature of 120 ˚C which over cures the PDMS and in the process helps bind the MLG nanoflakes to the inner pore walls. The deviation from linear behavior post ~ 2.18 N uniaxial loading can possibly be attributed to cell densification as discussed previously. Furthermore, the overcuring also stiffens the spongy PDMS base which can lead to a lesser sensitivity compared to our previous work [6]. The sensor demonstrates saturation from uniaxial compressive loading exceeding 4 N which can be attributed to the cell densification characteristics regime observed previously in the stress-strain characteristics curve.

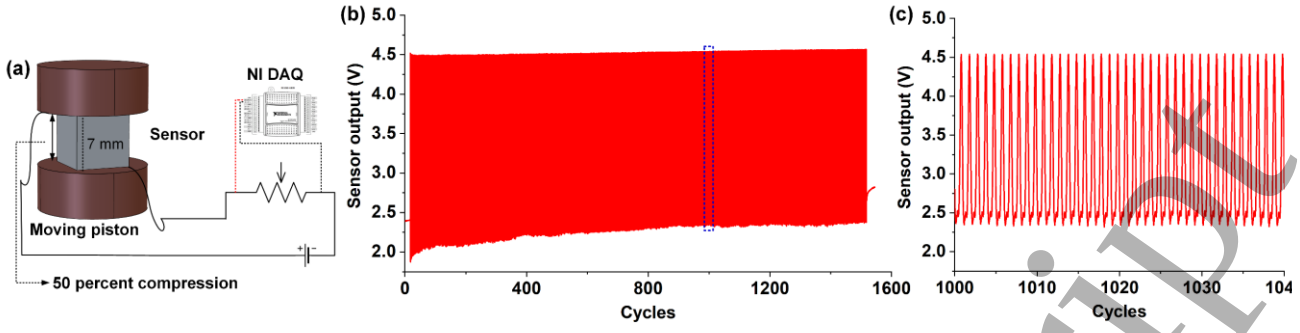

Figure 7. Accelerated lifetime test for the purpose of demonstrating reliability of the sensors: (**a**) Schematic representation of the experimental setup used for the accelerated lifetime test; (**b**) Plot showing sensor voltage response over 1500 cycles of repetitive uniaxial compressive loading; (**c**) Zoomed in plot showing the sensor voltage response.

To demonstrate the repetitive behavior of the sponges irrespective of the loading rate/frequency, two additional cyclic uniaxial compressive loading tests were conducted at 0.2 and 0.3 Hz frequencies. The blue lines of the plots in figure 5a,b, and c show the average baseline resistance of the sensor over the course of the calibration experiments. A slight change is baseline resistance is observed which can arise due to partial displacement of the MLG nanoflakes within the percolation network. The red lines of the plots in figure 5a,b, and c show the average resistance of the sensor under various compressive loadings for the three aforementioned frequencies which further consolidates the evidence of the linear nature of the sponges upto uiaxial loading of 2.18 N. The plots in figure 5d,e, and f show the normalized resistance change versus uniaxial compressive loading for 0.1, 0.2, and 0.3 Hz frequencies. Furthermore, the force sensitivities of the sponges were determined as 0.3068 N^{-1} , 0.2389 N^{-1} and 0.2451 N^{-1} at 0.1, 0.2, and 0.3 Hz cyclic uniaxial compressive loadings with R-squared values of 0.9925, 0.9962, and 0.9920 respectively. The behavior of the sponge remains predictable irrespective of the stimulus frequency which emphasizes its feasibility further for application involving wearable devices.

3.2 Evaluation of repeatability and accelerated lifetime performance

Repeatability is a critical parameter which is often overlooked and underreported in literature. However, process repeatability is of paramount importance when the fabricated sensors are intended for human motion monitoring and allied applications. To demonstrate the repeatability of our proposed fabrication process, three additional sensors were evaluated for cyclic compressive loading and their sensitivities and baseline resistances were measured at 0.2 Hz cyclic loading. The blue lines of the plots in figure 6a,b, and c show the average baseline resistance of the sensor over the course of the repeatability assessment experiments. As it is in the case of sensor 1, a slight shift in baseline resistance was observed over the course of the tests. The plots in figure 6d,e, and f show the normalized resistance change versus uniaxial compressive loading for sensors 2, 3, and 4 respectively. As clearly seen from the Baseline resistance change plots, all the sensors consistently demonstrate a baseline resistance variation which can possibly be attributed to a break-in phenomenon caused by settling graphene nanoflakes in the inner pore walls of the PDMS sponges. The sensors demonstrate a linear behavior in the compressive loading range ~ 0.42 – 2.18 N followed by a response saturation attributed to cell densification. Furthermore, the force sensitivities of the sensors 2, 3, and 4 were determined as 0.3725 N^{-1}, 0.4238 N^{-1}, and 0.3485 N^{-1} with R-squared values of 0.9878, 0.9803, and 0.9932 respectively. From the repeatability assessment tests, the mean force sensitivitiy of the sensors was determined as 0.3470 ± 0.0794 N^{-1} at 0.2 Hz cyclic compressive loading. All the sensors demonstrated a reproduceable linear response in the compressive load range ~ 0.42 – 2.18 N which is well within the typical force values exerted by human fingers on everyday objects like touchscreen. The results from the repeatability tests further assert our observation on the cell densification regime setting in post ~ 2.18 N uniaxial loading and subsequently all the sensor response tends toward sublinear behavior (for forces greater than 2.18 N). A study conducted by Asakawa et al. on 13 indivduals reported average loads of 0.5 N for tapping, 2.05 N for strectch, and 0.79 – 1.18 N for sliding gestures (using index and thumb fingers) [36]. Furthermore, applications involving detection of force exerted by shaving blades on the face are typically ~ 2 N [37] and thus underscores the applicability of our sensors for such smart products.

As the sensors proposed in this work are intended for real time human motion monitoring and applications involving wearables, the sensor was connected to a series variable resistance forming a matched voltage divider circuit as represented schematically in figure 7a. An accelerated lifetime

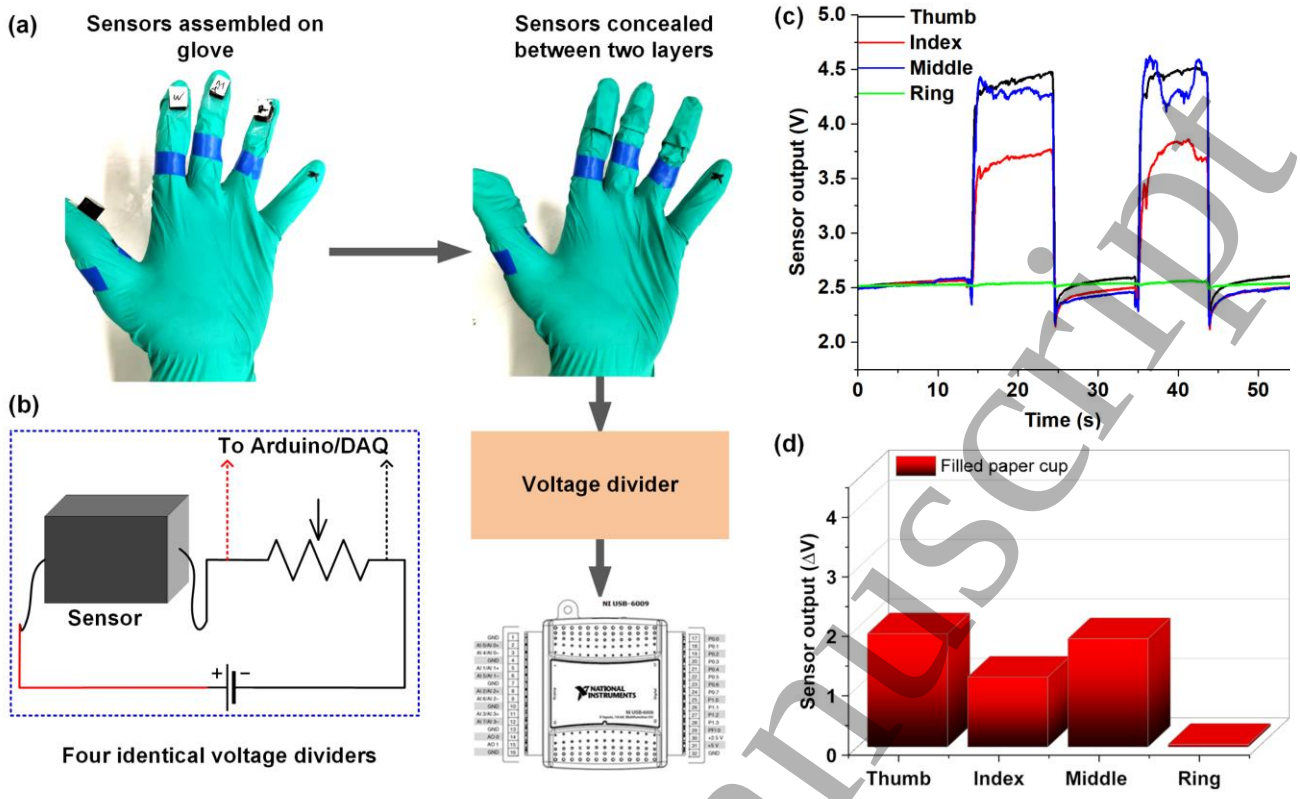

Figure 8. Application of the 3D graphene-PDMS sponges for a smart glove for IOT enabled grasping pressure monitoring: (**a**) Photograph showing four identical sensors secured on fingertip regions of a nitrile glove and subsequent encapsulation with a second nitrile layer; (**b**) Schematic representation of a simple voltage divider circuitry employed for acquiring the sensor response; (**c**) Plots showing the raw sensor(s) responses for grasping and releasing a filled paper cup twice; (d) Bar plot showing the average voltage response from the individual fingers while grasping a filled paper cup with three fingers.

test entailing 1500 cycles of repetitive uniaxial compressive loading (at 3.90 N) was conducted while the voltage signal from the voltage divider circuit was acquired continuously using NI USB-6009 DAQ system with accompanying Signal express software. The plot in figure 7b shows the voltage response over 1500 cycles of compressive strain loading. Figure 7c shows a zoomed-in version of the accelerated lifetime test in the range 1000 -1040 cycles.

The maximum drift in the voltage response is observed in the first 400 cycles of the accelerated life time assessment test. The observed drift can be attributed to two different underlying mechanisms. Firstly, the data acquisition circuit consists of a voltage divider circuit with a 0 - 5 kΩ series resistor which heats up during operation causing a resistance drift. Secondly, as observed from the comparison plots on the sensor baseline resistance drift in figure 6a-c, the break-in phenomenon causes an initial drift in sensor response. However, after the first 400 cycles, the drift is significantly reduced and the sensor baseline response changes from 2.2115 V (400th cycle) to 2.3796 V (1500th cycle). The sensor demonstrates a stable response over the duration of the test. The results of the accelerated lifetime assessment test in conjunction with process repeatability assessment tests underscore the reliability of our method and consolidates its applicability for applications involving wearables.

3.3 Smart glove for qualitative pressure monitoring

Recent progress in the development of flexible and soft sensors have enabled the next generation wearables, soft robotics, and devices with a capacity to recreate tactile sense through prosthetic artificial skins which function as large area tactile sensors similar to the human skin. The lightweight, squeezable, robust yet inexpensive nature of our graphene-PDMS sponges make them lucrative for applications involving tactile sensing and human motion monitoring. Furthermore, the sensor demonstrates a linear compressive load piezoresistive change characteristics in the range ~ 0.42 – 3.90 N which is well within the range of forces applied by human fingers while interacting with everyday objects like touchscreen interfaces [36]. Previously, we have

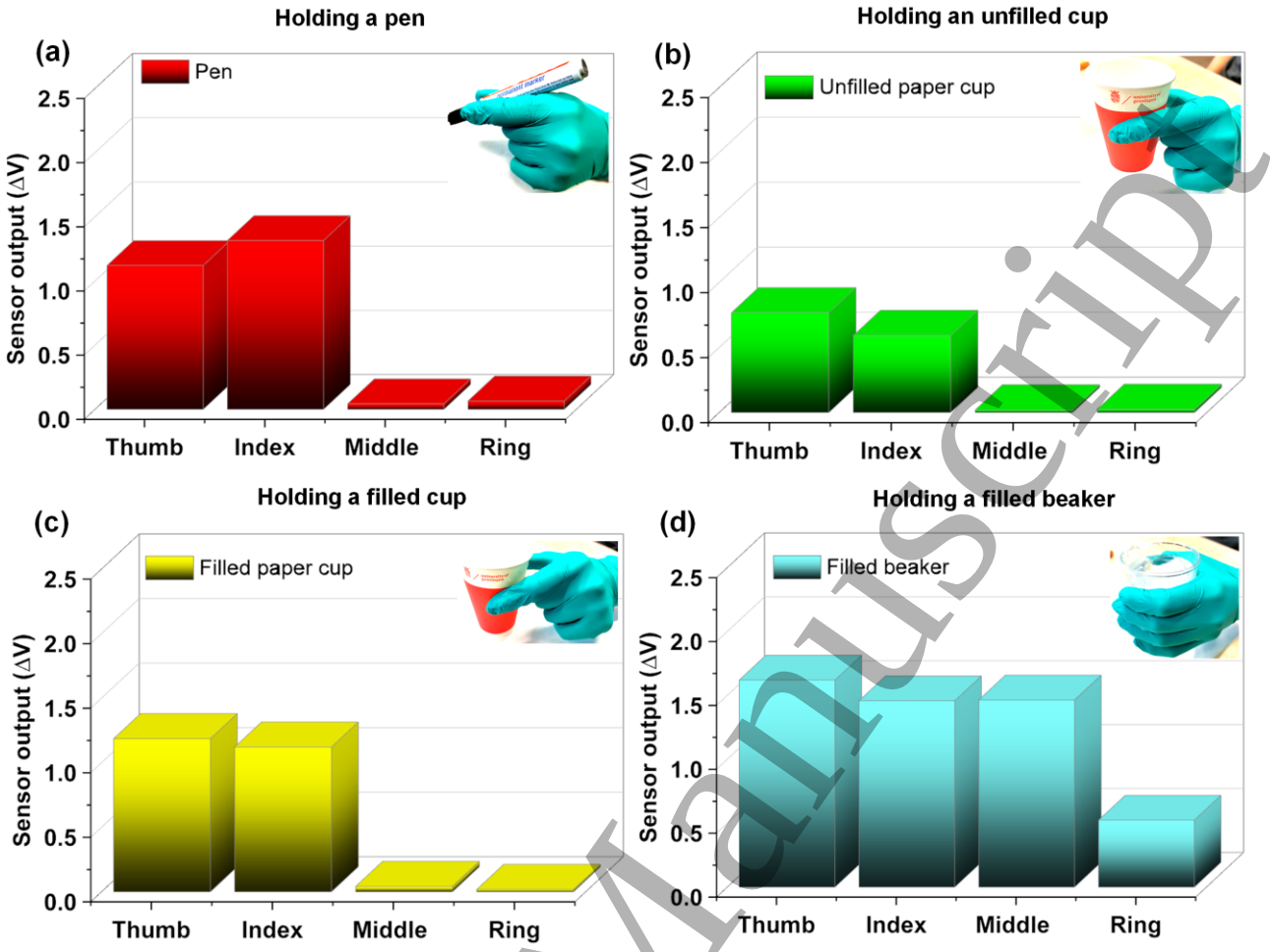

Figure 9. Grasping various objects used in day to day activities involving various fingers combinations: (**a**) Bar plot showing the average voltage response from the glove while grasping a pen with the thumb and index fingers; (**b**) Bar plot showing the average voltage response from the glove while grasping an unfilled paper cup with the thumb and index fingers; (**c**) Bar plot showing the average voltage response from the glove while grasping a filled paper cup with the thumb and index fingers; (**d**) Bar plot showing the average voltage response from the glove while grasping a filled beaker with the thumb, index, middle, and ring fingers.

demonstrated real-time gait and human motions monitoring employing similar sensors [6,33,44]. In this work, four identical graphene-PDMS sensors were employed for developing a pressure sensing glove for qualitative haptic pressure detection. Four identical electrically bonded graphene-PDMS sponges were affixed on the fingertip (thumb, index, middle, and ring fingers) regions of a soft nitrile glove. A second layer of nitrile was employed for covering the exposed sensors thus achieving a complete encapsulation protecting the sensors against external elements. Figure 8a shows the photographs of the sensors secured on a nitrile glove and subsequent encapsulation employing a second nitrile layer. The sensors were connected to four appropriately designed voltage divider circuits for converting the resistance change response to voltage signals. The voltage outputs were continuously logged employing NI USB-6009 data acquisition setup with accompanying signal express software.

A water filled paper cup was grabbed and released twice with three fingers (thumb, index, and middle fingers) and the voltage signals from the accompanying voltage divider circuits were logged continuously. The plot in figure 8c shows the raw signals from the sensors while grabbing the paper cup. For visual representation of qualitative relative pressure across the fingers, the peak changes in the signals were averaged for the entire duration of grabbing over the two cycles and a bar plot is drawn as shown in figure 8d. The bar plot provides a qualitative idea of the pressure distribution across the fingertips while holding an object.

Finally, to demonstrate the applicability of such systems in real life applications a human subject was made to put on the glove on left hand and grab various common everyday items. The response from the sensors were logged and converted to bar plots (employing the same method discussed earlier) to have a qualitative visualization of pressure distribution across

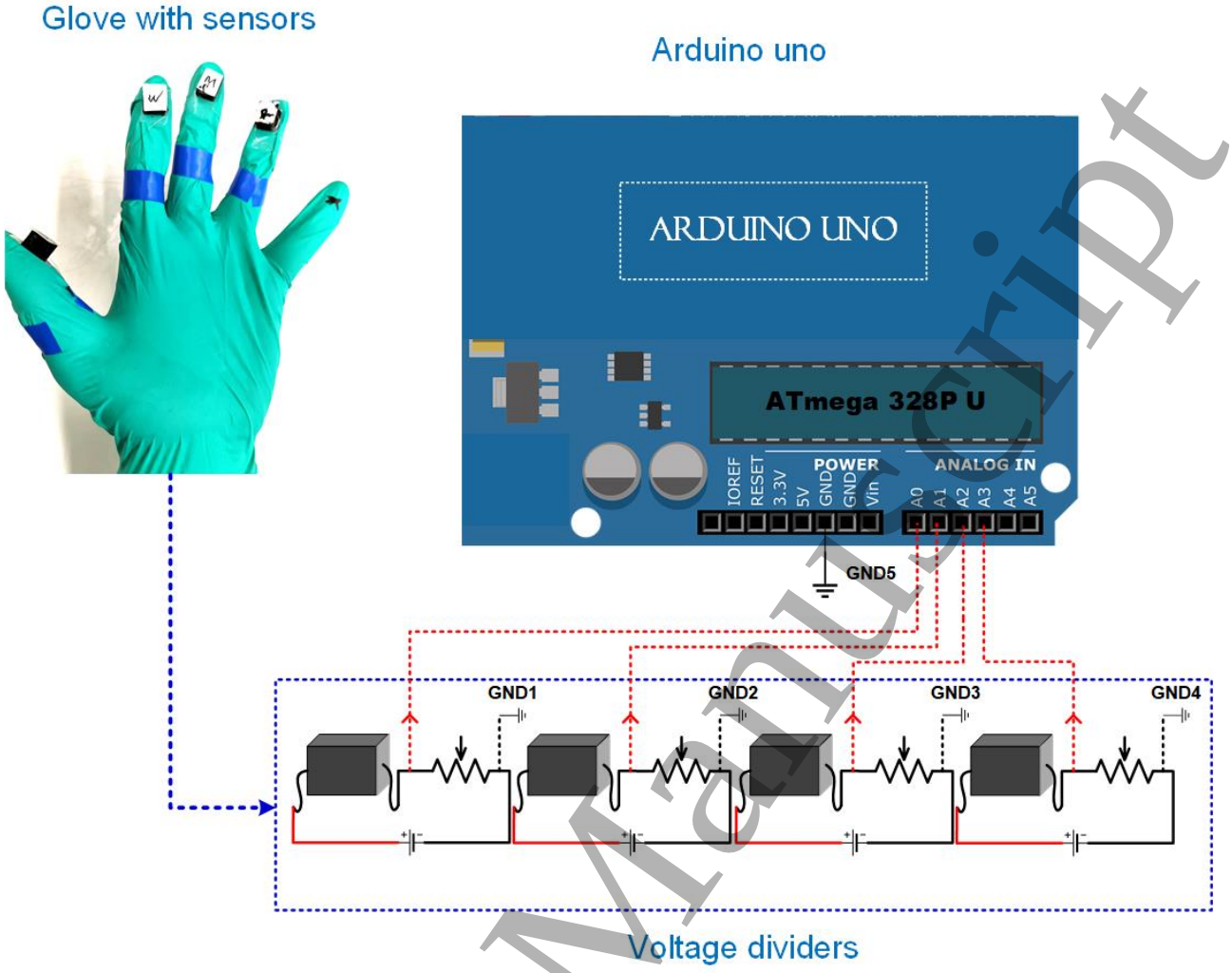

Figure 10. Arduino implementation for IOT applications: Schematic representation of the experimental setup involving the glove with accompanying voltage divider circuitry and an Arduino Uno board.

fingertips while holding the objects. Figure 9a-d show the bar plots from the individual fingers while holding a pen, an unfilled paper cup, a filled paper cup, and a filled glass beaker respectively. The photographs in the respective plot insets show the way in which the objects were grasped. As observed from the bar plots in figure 9b,c the system is able to discern between a filled cup and an unfilled cup.

In case of a filled cup more pressure is exerted on the fingertips while holding leading to a larger voltage output from the sensors. This trend is emphasized further while grabbing a relatively heavier filled beaker where all the fingers (thumb, index, middle and ring finger) exhibit higher voltage change implying relatively higher pressures being exerted on the fingertips. The grabbing exercise demonstrates the practicality of our sensors in system level implementation for applications involving smart wearables.

3.4 IoT implementation employing Arduino platform

The demand of IoT enabled wearable devices has grown exponentially over the past two decades with the availability of affordable beginner-friendly open-source microcontroller development board such as Arduino and Raspberry Pi. In the near future, IoT enabled wearable devices will facilitate remote health monitoring and telemedicine, robotics assisted remote surgical procedures, human-machine interface, and next generation prosthesis. To demonstrate the readiness of our device for next generation IoT/wireless applications, an embedded system comprising of the smart glove with readout voltage divider circuits and Arduino Uno platform is developed. The system is intended to display qualitative pressure information (in terms of four pressure levels namely, no pressure, low, medium, and high pressure respectively) while grasping objects. The schematic diagram in figure 10

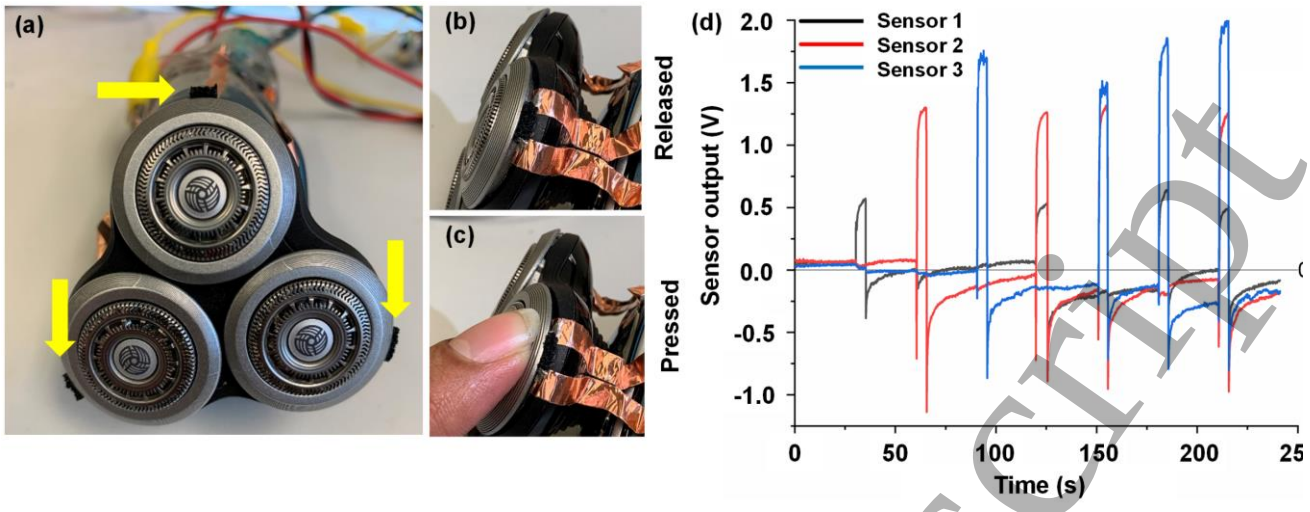

Figure 11. Sensorized shaver head for smart shaving application: (**a**) Three spongy sensors integrated under the three rotor caps of the Philips 9000 series shaver; (**b**) Rotor in the released state; (**c**) Rotor cap in the activated state; (**d**) Time series data of the three sensors for sequential activation of rotors in different combinations.

shows the circuit and connection diagram of the proposed system. The voltage divider outputs are connected to four analog input pins (A0, A1, A2, and A3) of the Arduino Uno board with a common ground configuration. All the four sensors were calibrated individually to display the following pressure levels: no pressure, low, medium, and high pressure. For real-time qualitative pressure distribution visualization, PLX-DAQ (Parallax Inc) software was used.

To demonstrate the real-time functioning of the system, the smart glove was worn, and a soft PU sponge was pressed with the index finger for three different pressure levels (low, medium and high pressure) for six seconds each, while the embedded system software displayed the qualitative pressure information in real-time (Supplementary video SV1). Furthermore, a filled beaker was grabbed while the embedded software displayed the qualitative pressure information across the four fingers tips (Supplementary video SV2). The embedded system implementation of the sensor system can be further extended for wireless acquisition protocol and demonstrates the feasibility of our sensor system for IoT enabled wearable and health care monitoring smart devices.

3.5 Sensor integration into electric shaver

The IoT revolution in the consumer goods market [45] has spurred the development of sensorized 'smart' products that operate with a high degree of autonomy and offer a tailored experience to the user. For instance, 'smart' shavers, such as the Philips 7000 series, wirelessly interface with a mobile app that provides customized guidance (depending upon skin type) to the male user during shaving, resulting in enhanced shaving comfort and reduced skin irritation, the latter bring a major dermatological complaint in American and European males [46]. Since shaving discomfort correlates with the force applied during shaving [46], it is desirable to measure the shaving forces, since the knowledge of these forces can be used to prompt the user (via the mobile app) to increase or decrease the magnitude of the applied force on the skin. Previous approaches in the literature utilized a single dome-shaped force sensor between the three rota cutting blades of the Philips shaver [47] to measure the average normal shaving force of the user. Here, we installed the spongy pressure sensors (sectioned into dimensions of approximately 5 mm × 3 mm × 3 mm) underneath the shaving caps of the three rota cutters as shown in Fig. 11a. This arrangement allowed us to determine which rotor was activated during shaving, an important consideration to ensure that the user adopts the suggested 'circular' shaving motion on the Philips rota shavers. Further, the sensor characterstics (i.e., linear behavior up to 2.18 N force, Fig. 3c) and low stiffness (~ 56.7 kPa, Fig. 3c) were ideal for the shaving application, since the former ensured that the sensors were capable of measuring the shaving forces (usually around ~ 2N [37]) while the latter ensured that the presenceof the sensor did not impede the tilting operation of the individual rotor caps.

The sensorized shaver head registered a response whenever one or more of the rotors were activated depending upon the strain state of the sensor, i.e. either released (Fig. 11b) or compressed (Fig. 11c), thus allowing a determination of the shaving pattern and forces of the individual user. As a proof of concept, we tested the sensorized shaver by manuallypressing (for 5 seconds) and activating the individual rotor caps every 30 seconds in the following sequence: 1, 2, 3, 1 and 2, 1 and 3, 2 and 3, and finally all of the rotor caps together (time series data shown in Fig. 11d). A video

demonstration of this test can be viewed in the Supplementary Video SV3. A follow-up test (Supplementary Video SV4) was conducted wherein a user was asked to mimic the shaving motion by sequentially touching the three rotor caps to his skin. The results indicated that the spongy sensors could successfully detect the sequential activation of one or more rota cutters, thus showing promise for next-generation smart shavers. For instance, based on the measured shaving pressure applied by the user, the smart shaving system can actuate mechanisms via which the skin-cutter distance, an important control parameter in shaving, can be maintained as close to zero as possible. Similarly, based on the observed shaving motion (inferred from the sequence of rotor actuation), the user can be prompted (via the mobile app) to adopt a more efficient motion to ensure a clean shave with minimal skin irritation.

4. Conclusion

In conclusion, we presented an improved facile recipe for fabricating linear and repeatable 3D porous graphene-PDMS piezoresistive sponges for smart wearable applications. In comparision with our previous work, the sensors developed in this work demonstrated more linear strain-resistance change response characteristics. Mechanical characterization tests revealed the ultralightweight nature of the sponges with a density of ~250 mg cm^{-3} and an elastic modulus of ~56.7 KPa. Electromechanical strain-resistance change response characterization experiments conducted on four identical sensors revealed a linear behavior for uniaxial compressive strains up to 2.18 N with an average force sensitivity of 0.3470 ± 0.0794 N^{-1}. Accelerated lifetime test entailing 1500 uniaxial compressive loading cycles (at 3.90 N) established long-term reliability and robust nature of the developed sensors. To establish the usability of the proposed sensor for smart wearable applications, a pressure sensing glove comprising of a soft nitrile glove with four identical graphene-PDMS sensors secured on the fingertip regions was developed and demonstrated for qualitative grasping pressure detection of daily life objects. Finally, the readiness and feasibility of the sensor system have been further emphasized through a custom-made embedded system (employing Arduino Uno platform) capable of real-time qualitative grasping pressure detection. The repeatable, robust, and ultralightweight nature of the sensor combined with the facile manufacturability make the proposed sensors suitable candidates for the development of next generation prosthetic devices for recreating the sense of touch in amputees, smart consumer products, and soft skin-like sensors for intelligent human-machine interfaces.

Author Contributions

Conceptualization, D.SG. and A.G.P.K.; methodology, D.S.G..; data collection and analysis, Q.F.S., D.S.G., and A.M.K; writing—original draft preparation, D.S.G.; writing—review and editing, A.G.P.K, B.J, and A.M.K.; supervision, A.G.P.K.

Funding

This research was supported by the University of Groningen's start-up grant awarded to A.G.P.K. Part of this work was labeled by ITEA and funded by local authorities under the grant agreement ITEA-2018-17030-Daytime.

Acknowledgment

The authors would like to thank Professor Yutao Pei from the department of Advanced production engineering, Univerity of Groningen for granting the access and training support for MTS 810 uniaxial testing setup and LYRA field-emission scanning electron.

Conflicts of Interest

The authors declare no conflict of interest.

References

[1] Sharma S, Chhetry A, Sharifuzzaman M, Yoon H and Park J Y 2020 Wearable Capacitive Pressure Sensor Based on MXene Composite Nanofibrous Scaffolds for Reliable Human Physiological Signal Acquisition *ACS Appl. Mater. Interfaces* **12** 22212–24

[2] Yang J, Luo S, Zhou X, Li J, Fu J, Yang W and Wei D 2019 Flexible, Tunable, and Ultrasensitive Capacitive Pressure Sensor with Microconformal Graphene Electrodes *ACS Appl. Mater. Interfaces* **11** 14997–5006

[3] Pang Y, Tian H, Tao L, Li Y, Wang X, Deng N, Yang Y and Ren T 2016 Flexible, Highly Sensitive, and Wearable Pressure and Strain Sensors with Graphene Porous Network Structure *ACS Appl. Mater. Interfaces* **8** 26458–62

[4] Sengupta D, Chen S, Michael A, Kwok C Y, Lim S, Pei Y and Kottapalli A G P 2020 Single and bundled carbon nanofibers as ultralightweight and flexible piezoresistive sensors *npj Flex. Electron.* **4** 9

[5] Amjadi M, Pichitpajongkit A, Lee S, Ryu S, Park I, Engineering M, Sensor M, Convergence I T and Korea S 2014 Highly Stretchable and Sensitive Strain Sensor Based on Silver Nanowire À Elastomer Nanocomposite 5154–63

[6] Sengupta D, Pei Y and Kottapalli A G P 2019 Ultralightweight and 3D Squeezable Graphene-Polydimethylsiloxane Composite Foams as Piezoresistive Sensors *ACS Appl. Mater. Interfaces* **11** 35201–11

[7] Choi W, Lee J, Kyoung Yoo Y, Kang S, Kim J and Hoon Lee J 2014 Enhanced sensitivity of piezoelectric pressure sensor with microstructured polydimethylsiloxane layer *Appl. Phys. Lett.* **104** 123701

[8] Hosseini E S, Manjakkal L, Shakthivel D and Dahiya R 2020 Glycine-Chitosan-Based Flexible Biodegradable Piezoelectric Pressure Sensor *ACS Appl. Mater. Interfaces* **12** 9008–16

[9] Sharma T, Je S S, Gill B and Zhang J X J 2012 Patterning piezoelectric thin film PVDF-TrFE based pressure sensor for catheter application *Sensors Actuators, A Phys.* **177** 87–92

[10] Ren Z, Nie J, Shao J, Lai Q, Wang L, Chen J, Chen X and Wang Z L 2018 Fully Elastic and Metal-Free Tactile Sensors for Detecting both Normal and Tangential Forces Based on Triboelectric Nanogenerators *Adv. Funct. Mater.*

[11] Tao J, Bao R, Wang X, Peng Y, Li J, Fu S, Pan C and Wang Z L 2019 Self-Powered Tactile Sensor Array Systems Based on the Triboelectric Effect *Adv. Funct. Mater.* **29** 1806379

[12] Charara M, Luo W, Saha M C and Liu Y 2019 Investigation of Lightweight and Flexible Carbon Nanofiber/Poly Dimethylsiloxane Nanocomposite Sponge for Piezoresistive Sensor Application *Adv. Eng. Mater.* **21** 1801068

[13] Rinaldi A, Tamburrano A, Fortunato M and Sarto M 2016 A Flexible and Highly Sensitive Pressure Sensor Based on a PDMS Foam Coated with Graphene Nanoplatelets *Sensors* **16** 2148

[14] Zhang S, Liu H, Yang S, Shi X, Zhang D, Shan C, Mi L, Liu C, Shen C and Guo Z 2019 Ultrasensitive and Highly Compressible Piezoresistive Sensor Based on Polyurethane Sponge Coated with a Cracked Cellulose Nanofibril/Silver Nanowire Layer *ACS Appl. Mater. Interfaces* **11** 10922–32

[15] Ryu S, Lee P, Chou J B, Xu R, Zhao R, Hart A J and Kim S-G 2015 Extremely Elastic Wearable Carbon Nanotube Fiber Strain Sensor for Monitoring of Human Motion *ACS Nano* **9** 5929–36

[16] Amjadi M, Yoon Y J and Park I 2015 Ultra-stretchable and skin-mountable strain sensors using carbon nanotubes–Ecoflex nanocomposites *Nanotechnology* **26** 375501

[17] Li Q, Liu H, Zhang S, Zhang D, Liu X, He Y, Mi L, Zhang J, Liu C, Shen C and Guo Z 2019 Superhydrophobic Electrically Conductive Paper for Ultrasensitive Strain Sensor with Excellent Anticorrosion and Self-Cleaning Property *ACS Appl. Mater. Interfaces* **11** 21904–14

[18] Cai J, Chawla S and Naraghi M 2014 Piezoresistive effect of individual electrospun carbon nanofibers for strain sensing *Carbon N. Y.* **77** 738–46

[19] Amjadi M, Pichitpajongkit A, Lee S, Ryu S and Park I 2014 Highly Stretchable and Sensitive Strain Sensor Based on Silver Nanowire–Elastomer Nanocomposite *ACS Nano* **8** 5154–63

[20] Yamada T, Hayamizu Y, Yamamoto Y, Yomogida Y, Izadi-Najafabadi A, Futaba D N and Hata K 2011 A stretchable carbon nanotube strain sensor for human-motion detection *Nat. Nanotechnol.* **6** 296–301

[21] Zhao J, He C, Yang R, Shi Z, Cheng M, Yang W, Xie G, Wang D, Shi D and Zhang G 2012 Ultra-sensitive strain sensors based on piezoresistive nanographene films *Appl. Phys. Lett.* **101** 063112

[22] Qin Y, Peng Q, Ding Y, Lin Z, Wang C, Li Y, Xu F and Li J 2015 Mechanically Flexible Graphene / Polyimide Nanocomposite Foam for Strain Sensor Application 8933–41

[23] Li L, Fu X, Chen S, Uzun S, Levitt A S, Shuck C E, Han W and Gogotsi Y 2020 Hydrophobic and Stable MXene–Polymer Pressure Sensors for Wearable Electronics *ACS Appl. Mater. Interfaces* **12** 15362–9

[24] Ma Y, Liu N, Li L, Hu X, Zou Z, Wang J, Luo S and Gao Y 2017 A highly flexible and sensitive piezoresistive sensor based on MXene with greatly changed interlayer distances *Nat. Commun.* **8** 1207

[25] Nguyen D D, Tai N-H, Lee S-B and Kuo W-S 2012 Superhydrophobic and superoleophilic properties of graphene-based sponges fabricated using a facile dip coating method *Energy Environ. Sci.* **5** 7908

[26] Liu H, Dong M, Huang W, Gao J, Dai K, Guo J, Zheng G, Liu C, Shen C and Guo Z 2017 Lightweight conductive graphene/thermoplastic polyurethane foams with ultrahigh compressibility for piezoresistive sensing *J. Mater. Chem. C* **5** 73–83

[27] Kamat A M and Kottapalli A G P 2021 3D Printed Graphene-Coated Flexible Lattice as Piezoresistive Pressure Sensor *2021 21st International Conference on Solid-State Sensors, Actuators and Microsystems (Transducers)* (IEEE) pp 888–91

[28] Hu H, Zhao Z, Wan W, Gogotsi Y and Qiu J 2013 Ultralight and Highly Compressible Graphene Aerogels *Adv. Mater.* **25** 2219–23

[29] Cao M, Su J, Fan S, Qiu H, Su D and Li L 2021 Wearable piezoresistive pressure sensors based on 3D graphene *Chem. Eng. J.* **406** 126777

[30] Chun S, Hong A, Choi Y, Ha C and Park W 2016 A tactile sensor using a conductive graphene-sponge composite *Nanoscale* **8** 9185–92

[31] Rinaldi A, Tamburrano A, Fortunato M and Sarto M 2016 A Flexible and Highly Sensitive Pressure Sensor Based on a PDMS Foam Coated with Graphene Nanoplatelets *Sensors* **16** 2148

[32] Tran D N H, Kabiri S, Sim T R and Losic D 2015 Selective adsorption of oil–water mixtures using polydimethylsiloxane (PDMS)–graphene sponges *Environ. Sci. Water Res. Technol.* **1** 298–305

[33] Sengupta D and Prakash Kottapalli A G 2020 Ultralight Weight Piezoresistive Spongy Graphene Sensors for Human Gait Monitoring Applications (Institute of Electrical and Electronics Engineers (IEEE)) pp 120–3

[34] Yan C, Wang J, Kang W, Cui M, Wang X, Foo C Y, Chee K J and Lee P S 2014 Highly Stretchable Piezoresistive Graphene–Nanocellulose Nanopaper for Strain Sensors *Adv. Mater.* **26** 2022–7

[35] Jing Z, Zhang Q, Cheng Y, Ji C, Zhao D, Liu Y, Jia W, Pan S and Sang S 2020 Highly sensitive, reliable and flexible piezoresistive pressure sensors based on graphene-PDMS @ sponge *J. Micromechanics Microengineering* **30** 085012

[36] Asakawa D S, Crocker G H, Schmaltz A and Jindrich D L 2017 Fingertip forces and completion time for index finger and thumb touchscreen gestures *J. Electromyogr. Kinesiol.* **34** 6–13

[37] Cowley K and Vanoosthuyze K 2016 The biomechanics of blade shaving *Int. J. Cosmet. Sci.* **38** 17–23

[38] Anon Poly(dimethylsiloxane)

[39] Sengupta D, Pei Y and Kottapalli A G P 2019 Ultralightweight and 3D Squeezable Graphene-Polydimethylsiloxane Composite Foams as Piezoresistive Sensors *ACS Appl. Mater. Interfaces* **11**

[40] Ashby M . 2005 The properties of foams and lattices *Philos. Trans. R. Soc. A Math. Phys. Eng. Sci.* **364** 15–30

[41] Wang Z, Volinsky A A and Gallant N D 2014 Crosslinking effect on polydimethylsiloxane elastic modulus measured by custom-built compression instrument *J. Appl. Polym. Sci.* **131**

[42] Maconachie T, Leary M, Lozanovski B, Zhang X, Qian M, Faruque O and Brandt M 2019 SLM lattice structures: Properties, performance, applications and challenges *Mater. Des.* **183** 108137

[43] Wu X, Han Y, Zhang X, Zhou Z and Lu C 2016 Large-Area Compliant, Low-Cost, and Versatile Pressure-

Sensing Platform Based on Microcrack-Designed Carbon Black@Polyurethane Sponge for Human–Machine Interfacing *Adv. Funct. Mater.* **26** 6246–56

[44] Sengupta D, Muthuram V and Prakash Kottapalli A G 2020 Flexible Graphene-on-PDMS Sensor for Human Motion Monitoring Applications *2020 IEEE SENSORS* (IEEE) pp 1–4

[45] Anon IoT Consumer Market Trends for 2020 - ASME

[46] Elsner P 2012 Overview and trends in male grooming *Br. J. Dermatol.* **166** 2–5

[47] Kamat A M, Pei Y, Jayawardhana B and Kottapalli A G P 2021 Biomimetic Soft Polymer Microstructures and Piezoresistive Graphene MEMS Sensors Using Sacrificial Metal 3D Printing *ACS Appl. Mater. Interfaces* **13** 1094–104